

Luminescent and Raman study of nanostructures formed upon annealing of SiO_x:Sm films

K.V. Michailovska, I.Z. Indutnyi, P.E. Shepeliavyi, M.V. Sopinsky, V.A. Dan'ko, V.O. Yukhymchuk

V. Lashkaryov Institute of Semiconductor Physics, NAS of Ukraine, 41, prosp. Nauky, 03680 Kyiv, Ukraine
Corresponding author e-mail: danko-va@ukr.net

Abstract. ncs-Si-SiO_x:Sm structures formed by high-temperature air annealing of the SiO_x films doped with samarium during thermal co-evaporation in vacuum of silicon monoxide and metallic Sm was studied. By measuring the spectra of photoluminescence (PL), it has been shown that doping of SiO_x films with Sm stimulates their decomposition into Si and SiO₂, and also reduces the transition temperature of silicon nanoparticle from the amorphous state to the crystalline one. With an increase in the impurity content up to 2 wt.%, along with the ncs-Si luminescence, the PL spectrum exhibits emission bands of Sm³⁺ and Sm²⁺ ions, which do not appear at a lower Sm concentration. The presence of silicon nanocrystals in SiO_x films doped with Sm and annealed at 970 °C in air has been confirmed using Raman scattering spectra. A possible mechanism for interaction of samarium ions with the SiO_x matrix and ncs-Si has been discussed.

Keywords: silicon nanoparticles, silicon nanocomposites, rare-earth, photoluminescence, Raman spectra, samarium.

<https://doi.org/10.15407/spqeo26.01.068>

PACS 78.30.Am, 78.60.Lc, 78.66.-w, 78.67.Bf, 78.67.-n

Manuscript received 28.06.22; revised version received 25.01.23; accepted for publication 08.03.23; published online 24.03.23.

1. Introduction

Silicon-oxide nanocomposites (ncs-Si-SiO_x, where ncs-Si – amorphous or crystalline silicon nanoparticles) doped with lanthanide (Ln) ions are of particular interest due to their promising application in modern photonic, optoelectronic, photovoltaic *etc.* devices that are compatible with mainstream microelectronic processing technology [1–6]. This is due to the fact that Ln ions in these structures display sharp or broad emission bands in the ultraviolet, visible and near-infrared spectral ranges. The absorption cross-section of ncs-Si exceeds that of direct excitation of Ln ions by almost three orders of magnitude [7, 8]. Accordingly, the ncs-Si-SiO_x structures doped with lanthanide ions can take advantage of the energy transfer from Si-nanoclusters to doping ions.

Most of the studies have been carried out on the ncs-Si-SiO_x structures doped with Er (see, for example, reviews [2, 3, 6]), and a number of works have been devoted to studying the luminescence properties of the structures doped with Tb [9–12], Nd [13–17], Ce [18–20], Tm [21, 22], Eu [23], Sm [24]. ncs-Si-SiO_x based nanocomposites doped with samarium are among the least studied ones. However, in our opinion, more attention should be paid to the formation and properties of ncs-Si-SiO_x structures doped with samarium, as well as the relationship between the emission characteristics

of samarium ions and the structure of the nanocomposites. As reported, in ncs-Si-SiO_x:Sm structures prepared using the oxygen annealing of the films obtained by the radio-frequency sputtering of the solid Si target partially covered with a layer of Sm₂O₃, samarium ions can take both 3⁺ and 2⁺ valence state [24]. It is known that emission spectrum of Sm³⁺ ions includes groups of lines within the range of 550...720 nm due to transitions from the ⁴G_{5/2} excited state to the ⁶H_{5/2}, ⁶H_{7/2}, ⁶H_{9/2}, and ⁶H_{11/2} levels [25]. Also, in some cases emission near 550...560 nm can be caused by the transition from the ⁴G_{7/2} to the ⁶H_{9/2} level [26]. The luminescence spectrum of Sm²⁺-doped phosphors usually consists of intense narrow lines within the range from 680 up to 830 nm attributed to ⁵D₀ → ⁷F_{*j*} (*j* = 0, 1, ... 4) transitions in the 4f⁶ configuration and one 4f⁵5d¹–4f⁶ broad band [27, 28]. Thus, doping with samarium allows large variability in the emission spectrum of the resulting phosphors.

Several authors have reported on the effects of metal impurities on the thermally stimulated decomposition of SiO_x, as well as on formation and crystallization of silicon nanoparticles in an oxide matrix [29–33]. In particular, the authors [32] demonstrated the stimulating effect of Er impurity on the nucleation and growth of Si nanocrystal during thermal treatment of SiO_x:Er films deposited using reactive sputtering in Ar/O₂ atmosphere of a silicon target partially covered

with metallic Er. The authors [34–36] found that air-annealing of $\text{SiO}_x:\text{Er},\text{F}$ films obtained by co-evaporation of SiO and ErF_3 results in more intense crystallization of a-Si nanoparticles and more perfect structure of the oxide matrix as compared to the similar annealing of evaporated SiO_x films. This dictates the need to study the effect of doping with samarium on the thermally stimulated decomposition of SiO_x , formation and crystallization of silicon nanoparticles in the oxide matrix.

In this work, the effect of samarium on the thermally stimulated decomposition of SiO_x during high-temperature annealing, formation of ncs-Si and their crystallization was studied by measuring the photoluminescence (PL) and Raman scattering (RS) spectra. A possible mechanism of thermally stimulated interaction of Sm ions with the SiO_x matrix and ncs-Si has been discussed.

2. Experimental procedure

The studied $\text{SiO}_x:\text{Sm}$ structures were obtained using thermal co-evaporation of silicon monoxide (Cerac Inc., Milwaukee, Wisconsin, USA) and metallic Sm powders in a vacuum of $\sim 10^{-3}$ Pa onto silicon wafers and sapphire substrates in a vertical evaporation geometry. The evaporation rate was monitored *in situ* by using two calibrated quartz microbalance. The Sm concentration in the samples varied from 0.8 up to 2.0 wt.%. The reference SiO_x films were deposited under the same conditions. The thickness of the obtained samples was measured after deposition using an MII-4 micro-interferometer and was 300...400 nm. Thermal treatment of the films after deposition was carried out at 500, 700 and 970 °C for 30 min in a silica furnace in air. As a result, the phase decomposition of the non-stoichiometric silicon oxide and the growth of ncs-Si in the oxide matrix occur.

The PL spectra were excited by linearly polarized laser diode radiation (wavelength 405 nm) at almost

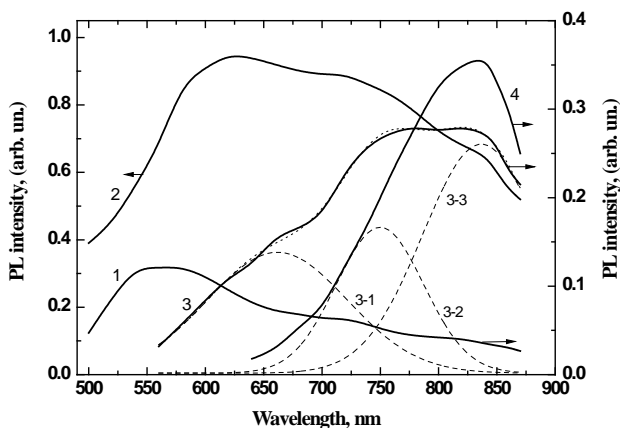


Fig. 1. Photoluminescence spectra of the $\text{SiO}_x:\text{Sm}$ film with the Sm concentration of 0.8 wt.% on the c-Si substrate: after deposition (1) and after annealing in air for 30 min at 500 (2), 700 (3), and 970 °C (4). Excitation by radiation with $\lambda = 405$ nm.

normal incidence on the surface of the samples. The emitted light was collected in the direction normal to the surface by using focusing lenses on the entrance slit of a ZMR-3 monochromator (spectral resolution ~ 1.2 nm for the 10- μm slit within the investigated wavelength range from 500 up to 1100 nm). The FEU-62 photomultiplier and a 232B synchronizing nanovoltmeter were used to record the PL signal. The PL spectra were measured at room temperature, and the spectral response of the detection system was corrected using the spectrum of a standard tungsten lamp. The structural characteristics of the samples were studied by analyzing the Raman spectra at room temperature. RS were excited by emission of Ar^+ laser (wavelength 457 nm) and recorded using a Horiba Jobin-Yvon T-64000 Raman spectrometer coupled to a high-sensitive CCD.

3. Results and discussion

Fig. 1 shows the PL spectra of SiO_x films on c-Si substrates with the samarium concentration 0.8 wt.%: as-deposited (1) and annealed at 500 (2), 700 (3) and 970 °C (4) for 30 minutes. The film without heat treatment (as-deposited) exhibits relatively weak PL emission with a maximum at about 560 nm, which is most likely associated with structural defects. After annealing at 500 °C, a significant increase in the PL intensity of the film is observed. Its emission in visible range spectrum is described by a wide non-elementary band as shown in Fig. 1 by curve 2. An increase in the annealing temperature (T_{an}) up to 700 °C causes some decrease in the PL intensity and a red shift of the band (Fig. 1, curve 3). Decomposition of this spectrum into three component bands using Gaussian functions is shown by dashed curves 3-1, 3-2 and 3-3. The PL emission of the short-wavelength band (curve 3-1) is usually associated with recombination on oxygen dangling bonds (nonbridging oxygen hole centers, NBOHCs) of the SiO_x matrix [37]. The emission spectrum presented by the curve 3-2 can be interpreted as the luminescence of amorphous silicon nanoclusters, which are formed in SiO_x films at medium annealing temperatures ($T_{an} < 900$ °C) and emit within the range 700...750 nm [38, 39]. The long-wave band represented by the curve 3-3 has a characteristic peak centered at 840 nm. The origin of this peak is usually associated with exciton recombination inside crystalline ncs-Si due to quantum confinement [40]. With a further increase in T_{an} to 970 °C (curve 4), a noticeable increase in the intensity of this PL band is observed, and the short-wave band due to NBOHCs completely disappears.

The luminescence spectra of the $\text{SiO}_x:\text{Sm}$ samples with the Sm concentration 1.5 wt.% are shown in Fig. 2. After annealing at $T_{an} = 500$ °C, the PL spectrum clearly shows the band with its maximum at 630 nm (curve 1), and at $T_{an} = 700$ °C, two overlapping bands appear with their maxima at 720 and 880...890 nm (curve 2). As mentioned above, these bands are associated with recombination of non-equilibrium carriers or excitons

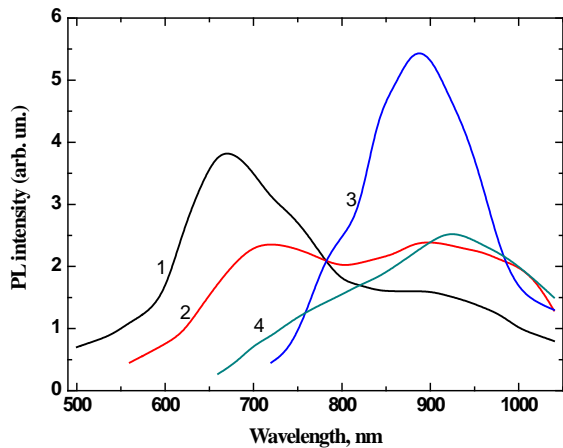


Fig. 2. Photoluminescence spectra of the $\text{SiO}_x\text{:Sm}$ samples with Sm concentration of 1.5 wt.% on the c-Si substrate after annealing in air for 30 min at 500 (1), 700 (2) and 970 °C (3). Excitation by radiation with $\lambda = 405$ nm. The curve 4: PL spectrum of non-doped SiO_x film annealed under the same conditions at 970 °C.

in amorphous and crystalline silicon nanoparticles or at their surface. When T_{an} increases to 970 °C, an increase in the intensity of the long-wave PL band is observed (Fig. 2, curve 3). It indicates that the amount of nanocrystalline silicon in the $\text{SiO}_x\text{:Sm}$ film also increases after annealing at a higher temperature. It should be noted that the Gaussian shape of this band and the spectral position of its maximum are close to the characteristics of the PL band observed in SiO_x films annealed at $T_{an} \geq 1100$ °C in argon atmosphere [41].

For comparison, Fig. 2 also shows the PL spectrum of the SiO_x film without samarium on the c-Si substrate after annealing under the same conditions at 970 °C (curve 4). The spectrum of the undoped SiO_x film covers the range from 650 up to 1050 nm, which corresponds to the luminescence of amorphous and amorphous-crystalline silicon nanoclusters. The emission of the SiO_x film annealed in air is weaker than the PL of the $\text{SiO}_x\text{:Sm}$ film annealed under the same conditions. It indicates that the samarium impurity stimulates decomposition of silicon suboxide and formation of silicon nanoparticles during high-temperature annealing. As seen in Figs 1 and 2, PL within the range 840...900 nm, which indicates the presence of silicon nanocrystals, is observed after annealing the $\text{SiO}_x\text{:Sm}$ samples at 700 and even 500 °C. It indicates that the samarium impurity stimulates not only decomposition of SiO_x and formation of ncs-Si, but also promotes crystallization of amorphous silicon nanoparticles at lower annealing temperatures.

In the luminescence spectra of $\text{SiO}_x\text{:Sm}$ films with a high impurity content (2 wt %), along with the PL band of nanosilicon, emission bands of samarium ions (Sm^{3+} and Sm^{2+}) appear, too. Fig. 3 shows the PL spectra of such a film before and after annealing at 500 and 970 °C. In the non-annealed film, against the background of a weak PL signal, two bands with the maxima at 550 and 725 nm are observed (curve 1). These bands correlate

well with the spectral position of the emission bands of Sm^{3+} and Sm^{2+} ions in a glassy matrix [42]. In the film under study, the 550 nm band is close to the 560-nm emission band of Sm^{3+} ions, which corresponds to the $4f-4f$ shell transition of the samarium from the excited state to the ground state (${}^4G_{5/2} \rightarrow {}^6H_{5/2}$). In contrast to Sm^{3+} ions, the main emission bands of Sm^{2+} ions are somewhat redshifted. At room temperature, the 724 nm band usually appears, which corresponds to $4f^5 5d^1-4f^6$ shell transition of samarium from the excited state to the ground state (${}^5D_0 \rightarrow {}^7F_2$) [42, 43]. The spectral position of this band is in good agreement with the maximum of the PL band in the unannealed film at 725 nm (curve 1). Its large halfwidth is caused by the strong coupling of $5d$ electrons with lattice vibrations and the thermal population of the excited $4f^5 5d^1$ level. The density of states of the excited level of Sm^{2+} ions is higher as compared to the $4f-4f$ levels of Sm^{3+} ions, so the excitation spectrum of Sm^{2+} ions is much wider (the visible to ultraviolet band) [42, 43]. The source of excitation of all photoluminescence spectra used in the work was a laser diode with the emission wavelength 405 nm, corresponding to the absorption bands of Sm^{3+} and Sm^{2+} ions [44, 45].

After annealing the samples at $T_{an} = 500$ °C, the luminescence intensity noticeably increases, and its spectral composition covers the visible and near-IR spectral ranges (Fig. 3, curve 2). Decomposition of the PL spectrum into component bands (not shown) and their analysis enabled to associate these bands with formation of amorphous and amorphous-crystalline silicon nanocomposites. The luminescence bands of silicon nanocomposites, as well as the emission bands of Sm^{3+} and Sm^{2+} ions, are located in the orange-red region of the spectrum and overlap with each other, which somewhat complicates their identification. However, the presence of two shoulders at ~545 and ~600 nm on the short-wave side of the PL spectrum can be associated with manifestation of bands at 560 and 600 nm due to radiative

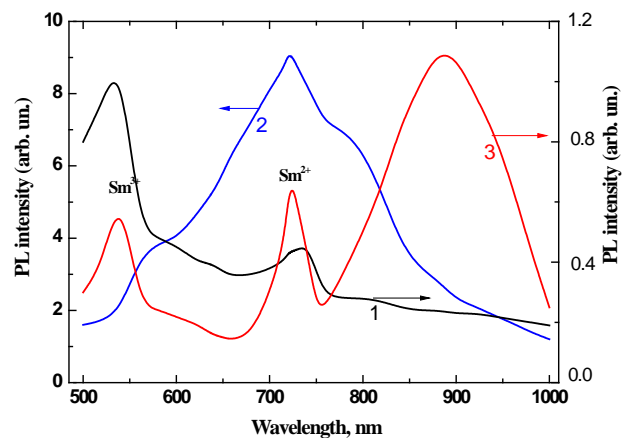


Fig. 3. Photoluminescence spectra of the $\text{SiO}_x\text{:Sm}$ samples with the Sm concentration of 2 wt.% on the c-Si substrate: as-deposited (1) and after annealing in air for 30 min at 500 (2), and 970 °C (3). Excitation by radiation with $\lambda = 405$ nm.

transitions in Sm^{3+} ions (${}^4\text{G}_{5/2} \rightarrow {}^6\text{H}_j$, $j = 5/2, 7/2$, respectively). The curve 2 also clearly shows a narrow peak at 725 nm and the shoulder at 780 nm, position of which correlates with the emission bands of Sm^{2+} ions at 728 and 766 nm [24].

Annealing of SiO_x films with 2 wt.% Sm (as well as samples with a lower impurity content) at $T_{\text{an}} = 970$ °C is accompanied by the transition of a significant part of silicon nanoparticles from the amorphous state to the crystalline one and the corresponding change in the PL spectrum. As a result, the radiation of amorphous nanosilicon is noticeably attenuated, and a broad band appears in the IR region of the spectrum with its maximum at ~ 910 nm for SiO_x films with 2 wt.% Sm, as shown in Fig. 3. Moreover, due to the transition of nanosilicon from the amorphous state to the crystalline one and the weakening of the PL signal in the orange-red range, the emission of Sm^{3+} and especially Sm^{2+} ions becomes more pronounced. It can be seen that, after annealing, the position of the bands maxima at 725 nm and at 550 nm does not change, but the ratio of their intensities changes (Fig. 3, curves 1 and 3). It is known that the ${}^5\text{D}_0 \rightarrow {}^7\text{F}_2$ electric dipole transition (~ 725 nm) is a very sensitive to ligand field and is often used as a sensitive probe of the electronic and structural properties of the host material [46, 47]. But the ${}^4\text{G}_{5/2} \rightarrow {}^6\text{H}_{5/2}$ magnetic dipole transition corresponding to the ~ 550 nm band is weakly sensitive to structural changes in the environment of Sm^{3+} ions [48]. Therefore, the observed change in the intensity ratio of the bands can be due to a change in the chemical composition of the Sm ions' environment during annealing.

If we consider the dependence of the luminescent properties of $\text{SiO}_x\text{:Sm}$ samples on the impurity concentration, we can note the following features. In samples annealed at 970 °C with an increase in the content of samarium from 0.8 to 2 wt.%, the shift of the maximum of the PL band of nanocrystalline silicon from 840 to 910 nm is observed. The PL intensity also changes: first it increases with an increase in the samarium concentration, and then decreases. The highest integrated PL intensity is observed in films with the Sm content close to 1.5 wt.%.

As the impurity content increases to 2 wt.%, along with the ncs-Si luminescence, emission bands of Sm^{3+} and Sm^{2+} ions appear in the PL spectrum, which, as seen from Figs 1 and 2, do not appear at a lower Sm content. It is known that in homogeneous matrices (crystals, glasses) the luminescence intensity of lanthanide ions is directly proportional to their concentration up to the onset of concentration quenching [43]. But we observe the threshold character of samarium ions PL. It indicates that a significant fraction of samarium ions in the $\text{SiO}_x\text{:Sm}$ structures is in the radiatively inactive form. The physical mechanism of such a concentration dependence of samarium impurity PL remains to be elucidated. It can be assumed that this is due to the heterogeneous nature of the matrix, which consists of silicon oxide and silicon inclusions. Therefore, a non-uniform distribution of samarium ions can be expected, and at lower ion

concentrations, their predominant fraction is in the regions that contribute to the quenching of their glow (for example, they passivate the ncs-Si surface).

The traditional method for detecting nanocrystalline silicon in annealed SiO_x films is Raman spectroscopy. Fig. 4 displays the $460\text{--}560\text{ cm}^{-1}$ frequency range of the Raman spectrum of the annealed at 970 °C $\text{SiO}_x\text{:Sm}$ film with Sm concentration of 1.5 wt.% on a sapphire substrate. In this frequency range, there are no lines characteristic of the Raman spectra of the sapphire substrate, which simplifies the processing of the obtained experimental data. At the same time, as it is known, the vibrational spectra of optical phonons (their transverse modes) corresponding to the amorphous ($\sim 480\text{ cm}^{-1}$) and crystalline ($\sim 521\text{ cm}^{-1}$) phases of silicon should be located in this frequency range. Deconvolution of the Raman spectrum showed that it consists of two Gaussian bands (dashed curves in Fig. 4). The first is a relatively sharp (halfwidth 12 cm^{-1}) band centered at the frequency 525.3 cm^{-1} (curve 1). Its presence confirms the results of luminescent measurements indicating the presence of silicon nanocrystals in the annealed film. Due to the size-induced confinement in Si nanocrystals, a red shift of the phonon band relative to the bulk phonon frequency of Si (521 cm^{-1}) should be observed [49]. However, in our case, there is a blue shift with respect to the phonon frequency of the Si macrocrystal. Mechanical strain or stress can affect Raman mode frequencies. The total shift towards higher frequencies indicates the existence of strong compressive stresses in Si nanocrystals, which act in the direction opposite to the phonon confinement effect [50]. Similar blueshifted Raman spectra of Si nanocrystals were observed in $\text{SiO}_x\text{:Er,F}$ films on sapphire substrates, which were also annealed in air [39]. In such samples, all three possible contributions to the total stress (external stress, intrinsic stress, and thermal stress) for Si nanocrystals are of a compressive nature [39].

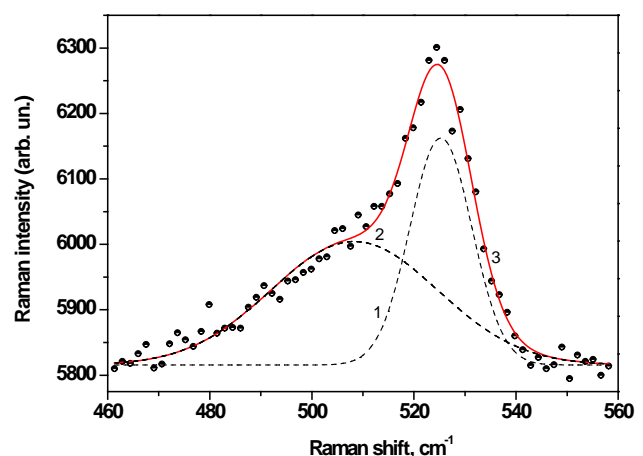


Fig. 4. Raman spectrum of the $\text{SiO}_x\text{:Sm}$ sample with the Sm concentration of 1.5 wt.% on the sapphire substrate after annealing in air for 30 min at 970 °C (dots – the results of experiment). The red line (3) is the result of superposition of the Gaussian curves 1 and 2.

The second band in the Raman spectrum has a maximum at 508.3 cm^{-1} and the halfwidth of 32 cm^{-1} (curve 2). The Si phonon frequencies within the range $495\text{--}510\text{ cm}^{-1}$ have been attributed to the interface of smaller size silicon nanocrystals and SiO_2 matrix [51]. At the same time, we do not observe a signal from the a-Si TO mode. This indicates the absence of a clearly defined amorphous silicon phase (possibly, non-crystalline silicon is in a strongly dispersed form). Its absence is also indicated by the luminescence spectrum (not shown) of the same films, in which the PL band characteristic of amorphous silicon is absent.

The above studies have shown that doping of SiO_x films with metallic samarium stimulates decomposition of silicon suboxide, formation and crystallization of silicon nanoparticles in the oxide matrix. In particular, the impurity lowers the transition temperature for conversion of silicon nanoparticles from amorphous to crystalline state. Similar results were obtained for SiO_x films doped, for example, with nickel [29], tin [31], erbium [32], aluminum [33], and ErF_3 [34–36]. It can be assumed that the mechanism of samarium-induced decomposition of SiO_x also includes the oxidation of the impurity Sm atoms by oxygen of the oxide matrix. When Sm interacts with oxygen of weakly oxidized molecular clusters of the SiO_x layer, such as $\text{Si}(\text{OSi}_3)$, for example, the latter can lose oxygen, which leads to a local increase in the Si concentration in the SiO_x matrix and stimulates formation of ncs-Si. It has been ascertained that samarium not only accelerates formation of ncs-Si, but also participates in the passivation of their surface. We suppose that the passivation of dangling bonds in $\text{SiO}_x\text{:Sm}$ films occurs in the oxide shell surrounding ncs-Si due to Si–O–Sm binding.

4. Conclusions

Thus, the effect of the samarium impurity and its concentration on formation of nanosized silicon in films of amorphous suboxide has been studied. By measuring the PL spectra, the influence of the samarium impurity on the acceleration of thermally stimulated decomposition of $\text{SiO}_x\text{:Sm}$ films into silicon and silicon oxide, as well as the acceleration of crystallization inherent to the formed amorphous silicon nanoparticles, has been ascertained. The presence of crystalline silicon nanoparticles in SiO_x films doped with samarium and annealed at $970\text{ }^\circ\text{C}$ is confirmed by the Raman spectra. It has been assumed that the mechanism of stimulation of SiO_x decomposition during annealing is due to the reaction of Sm atoms with oxygen of the oxide matrix, which leads to a local increase in the concentration of Si–Si bonds and nucleation of silicon particles near impurity atoms. Passivation of the ncs-Si surface due to Si–O–Sm bonds significantly slows down their additional oxidation with atmospheric oxygen during annealing in air.

In the samples with the impurity content close to 2 wt.%, along with the luminescence of ncs-Si, the emission bands of Sm^{3+} and Sm^{2+} ions appear in the PL spectrum. The concentration dependence of these bands exhibits threshold character: PL of samarium impurities does not appear at lower Sm concentrations.

References

1. Canham L. Introductory lecture: origins and applications of efficient visible photoluminescence from silicon-based nanostructures. *Faraday Discuss.* 2020. **222**. P. 10–81. <https://doi.org/10.1039/D0FD00018C>.
2. Pavesi L. Thirty years in silicon photonics: A personal view. *Front. Phys.* 2021. **9**. P. 786028. <https://doi.org/10.3389/fphy.2021.786028>.
3. *Silicon Nanophotonics: Basic Principles, Present Status, and Perspectives*. Second Edition. Ed. L. Khriachtchev. Pan Stanford Publishing, 2016.
4. Mazzaro R., Romano F., and Ceroni P. Long-lived luminescence of silicon nanocrystals: From principles to applications. *Phys. Chem. Chem. Phys.* 2017. **19**, No 39. P. 26507–26526. <https://doi.org/10.1039/C7CP05208A>.
5. Yuan Z., Anopchenko A., Pavesi L. Innovative quantum effects in silicon for photovoltaic applications. Ch. 10 in: *Advanced Silicon Materials for Photovoltaic Applications*. Ed. S. Pizzini. John Wiley & Sons, 2012. P. 355–391.
6. Sopinsky M., Khomchenko V. Electroluminescence in SiO_x films and SiO_x film-based systems. *Curr. Opin. Solid State Mater. Sci.* 2003. **7**, No 2. P. 97–109. [https://doi.org/10.1016/S1359-0286\(03\)00048-2](https://doi.org/10.1016/S1359-0286(03)00048-2).
7. Pacifici D., Franzò G., Priollo F., Iacona F., and Dal Negro L. Modeling and perspectives of the Si nanocrystals–Er interaction for optical amplification. *Phys. Rev. B.* 2003. **67**, No 24. P. 245301. <https://doi.org/10.1103/PhysRevB.67.245301>.
8. Pacifici D., Irrera A., Franzò G. *et al.* Erbium-doped Si nanocrystals: Optical properties and electroluminescent devices. *Physica E.* 2003. **16**, No 3–4. P. 331–340. [https://doi.org/10.1016/S1386-9477\(02\)00615-X](https://doi.org/10.1016/S1386-9477(02)00615-X).
9. Khomchenko V.S., Berejinskij L.I., and Sopinsky M.V. On the correlation character between the structure perfection and electroluminescent properties of terbium doped silicon monoxide films. *Physica B.* 2001. **308–310**. P. 268–271. [https://doi.org/10.1016/S0921-4526\(01\)00791-8](https://doi.org/10.1016/S0921-4526(01)00791-8).
10. Kaleli B., Kulacki M., Turan R. Mechanisms of light emission from terbium ions (Tb^{3+}) embedded in a Si rich silicon oxide matrix. *Opt. Mater.* 2012. **34**, No 11. P. 1935–1939. <https://doi.org/10.1016/j.optmat.2012.05.036>.
11. Kulacki M., Turan R. Improvement of light emission from Tb-doped Si-based MOS-LED using excess Si in the oxide layer. *J. Lumin.* 2013. **137**. P. 37–42. <https://doi.org/10.1016/j.jlumin.2012.11.005>.
12. Podhorodecki A., Golacki L.W., Zatyrb G. *et al.* Excitation mechanism and thermal emission quenching of Tb ions in silicon rich silicon oxide thin films grown by plasma-enhanced chemical vapour deposition – Do we need silicon nanoclusters? *J. Appl. Phys.* 2014. **115**, No 14. Art. 143510 (10 p.). <https://doi.org/10.1063/1.4871015>.

13. Debieu O., Cardin J., Portier X., Gourbilleau F. Effect of the Nd content on the structural and photoluminescence properties of silicon-rich silicon dioxide thin films. *Nanoscale Res. Lett.* 2011. **6**, No 1. P. 161. <https://doi.org/10.1186/1556-276X-6-161>.
14. Liang C.-H., Cardin J., Labbé C., Gourbilleau F. Evidence of two sensitization processes of Nd³⁺ ions in Nd-doped SiO_x films. *J. Appl. Phys.* 2013. **114**, No 3. P. 033103. <https://doi.org/10.1063/1.4813610>.
15. Khomenkova L., Labbé C., Portier X., Carrada M., Gourbilleau F. Undoped and Nd³⁺ doped Si-based single layers and superlattices for photonic applications. *phys. status solidi (a)*. 2013. **210**, No 8. P. 1532–1543. <https://doi.org/10.1002/pssa.201200942>.
16. Steveler E., Rinnert H., Vergnat M. Photoluminescence properties of Nd-doped silicon oxide thin films containing silicon nanoparticles. *J. Lumin.* 2014. **150**. P. 35–39. <https://doi.org/10.1016/j.jlumin.2014.01.061>.
17. Steveler E., Rinnert H., and Vergnat M. Low-temperature photoluminescence properties of Nd-doped silicon oxide thin films containing silicon nanocrystals. *J. Lumin.* 2017. **183**. P. 311–314. <https://doi.org/10.1016/j.jlumin.2016.11.048>.
18. Beainy G., Weimmerskirch-Aubatin J., Stoffel M. *et al.* Structural and optical study of Ce segregation in Ce-doped SiO_{1.5} thin films. *J. Appl. Phys.* 2015. **118**, No 23. P. 234308. <https://doi.org/10.1063/1.4938061>.
19. Beainy G., Weimmerskirch-Aubatin J., Stoffel M. *et al.* Atomic scale investigation of Si and Ce-rich nanoclusters in Ce-doped SiO_{1.5} thin films. *phys. status solidi (c)*. 2015. **12**, No 12. P. 1313–1316. <https://doi.org/10.1002/pssc.201510081>.
20. Beainy G., Weimmerskirch-Aubatin J., Stoffel M. *et al.* Direct insight into Ce-silicates/Si-nanoclusters snowman-like Janus nanoparticles formation in Ce-doped SiO_x thin layers. *J. Phys. Chem. C*. 2017. **121**, No 22. P. 12447–12453. <https://doi.org/10.1021/acs.jpcc.7b03199>.
21. Watanabe K., Tamaoka H., Fujii M. *et al.* Excitation of Tm³⁺ by the energy transfer from Si nanocrystals. *Physica B*. 2001. **308–310**. P. 1121–1124. [https://doi.org/10.1016/S0921-4526\(01\)00903-6](https://doi.org/10.1016/S0921-4526(01)00903-6).
22. Watanabe K., Tamaoka H., Fujii M., Moriwaki K., Hayashi S. Excitation of Nd³⁺ and Tm³⁺ by the energy transfer from Si nanocrystals. *Physica E*. 2002. **13**, No 2–4. P. 1038–1042. [https://doi.org/10.1016/S1386-9477\(02\)00297-7](https://doi.org/10.1016/S1386-9477(02)00297-7).
23. Li D., Zhang X., Jin L., Yang D. Structure and luminescence evolution of annealed Europium-doped silicon oxides films. *Opt. Exp.* 2010. **18**, No 26. P. 27191–27196. <https://doi.org/10.1364/OE.18.027191>.
24. Zanatta A.R. Coexistence of Sm³⁺ and Sm²⁺ ions in amorphous SiO_x: Origin, main light emission lines and excitation-recombination mechanisms. *Opt. Mater. Exp.* 2016. **6**, No 6. P. 2109–2117. <https://doi.org/10.1364/OME.6.002108>.
25. Dieke G.H. *Spectra and Energy Levels of Rare Earth Ions in Crystals*. Wiley, New York, 1968.
26. Kushnirenko V.I., Sopinskyy M.V., Manoilov E.G., Khomchenko V.S. Luminescent spectroscopy of TbF₃ and TbF₃–SmF₃–HoF₃–PrF₃ crystals. *J. Alloys. Compd.* 2008. **451**, No 1–2. P. 209–211. <https://doi.org/10.1016/j.jallcom.2007.04.178>.
27. Ofelt G.S. Structure of the f⁶ configuration with application to rare-earth ions. *J. Chem. Phys.* 1963. **38**, No 9. P. 2171–2179. <https://doi.org/10.1063/1.1733947>.
28. Grenet G., Kibler M., Gros A. *et al.* Spectrum of Sm²⁺:SrClF. *Phys. Rev. B*. 1980. **22**, No 11. P. 5052–5067. <https://doi.org/10.1103/PhysRevB.22.5052>.
29. He Y., Ma K., Bi L., Feng J.Y., Zhang Z.J. Nickel-induced enhancement of photoluminescence from Si-rich silica films. *Appl. Phys. Lett.* 2006. **88**, No 3. P. 031905. <https://doi.org/10.1063/1.2165292>.
30. Yoon J.H. Enhanced formation of Si nanocrystals in silicon-rich oxide implanted with Ni. *Mater. Lett.* 2014. **136**. P. 237–240. <https://doi.org/10.1016/j.matlet.2014.07.178>.
31. Voitovych V.V., Rudenko R.M., Kolosiuk A.G. *et al.* Effect of tin on the processes of silicon-nanocrystal formation in amorphous SiO_x thin-film matrices. *Semiconductors*. 2014. **48**, No 1. P. 73–76. <https://doi.org/10.1134/S1063782614010242>.
32. Mustafa D., Biggemann D., Martens J.A. *et al.* Erbium enhanced formation and growth of photoluminescent Er/Si nanocrystals. *Thin Solid Films*. 2013. **536**. P. 196–201. <https://doi.org/10.1016/j.tsf.2013.03.027>.
33. Zamchiy A.O., Baranov E.A., Khmel S.Ya. *et al.* Aluminum-induced crystallization of silicon suboxide thin films. *Appl. Phys. A*. 2018. **124**. P. 646. <https://doi.org/10.1007/s00339-018-2070-y>.
34. Vlasenko N.A., Sopinskii N.V., Gule E.G. *et al.* Effect of erbium fluoride doping on the photoluminescence of SiO_x films. *Semiconductors*. 2012. **46**, No 3. P. 323–329. <https://doi.org/10.1134/S1063782612030232>.
35. Nikolenko A.S., Sopinskii N.V., Strelchuk V.V. *et al.* Raman study of Si nanoparticles formation in the annealed SiO_x and SiO_x:Er,F films on sapphire substrate. *J. Optoelectron. Adv. Mater.* 2012. **14**, No 1–2. P. 120–124.
36. Sopinskii N.V., Vlasenko N.A., Lisovskyy I.P. *et al.* Formation of nanocomposites by oxidizing annealing of SiO_x and SiO_x(Er,F) films: Ellipsometry and FTIR analysis. *Nanoscale Res. Lett.* 2015. **10**. P. 232. <https://doi.org/10.1186/s11671-015-0933-0>.
37. Kenyon A.J., Trwoda P.F., Pitt C.W. The origin of photoluminescence from the thin films of silicon-rich silica. *J. Appl. Phys.* 1996. **79**, No 12. P. 9291–9299. <https://doi.org/10.1063/1.362605>.

38. Lisovskyy I.P., Indutnyy I.Z., Gnenny B.N. *et al.* Structural–phase transformations in SiO_x films in the course of vacuum heat treatment. *Semiconductors*. 2003. **37**, No 1. P. 97–102. <https://doi.org/10.1134/1.1538546>.
39. Indutnyi I.Z., Michailovska E.V., Shepeliavyi P.E., and Dan’ko V.A. Visible photoluminescence of selectively etched porous nc-Si–SiO_x structures. *Semiconductors*. 2010. **44**, No 2. P. 206–210. <https://doi.org/10.1134/S1063782610020120>.
40. Limpens R., Lesage A., Fujii M., Gregorkiewicz T. Size confinement of Si nanocrystals in multi-nanolayer structures. *Sci. Rep.* 2015. **5**. P. 17289. <https://doi.org/10.1038/srep17289>.
41. Lisovskyy I.P., Voitovich M.V., Sarikov A.V. *et al.* Transformation of the structure of silicon oxide during the formation of Si nanoinclusions under thermal annealing. *Ukr. J. Phys.* 2009. **54**, No 4. P. 383–390.
42. Malchukova E.V., Boizot B., Trapeznikova I.N., and Terukov E.I. Optical properties and kinetics of the luminescence decay of Sm³⁺ and Sm²⁺ ions in aluminoborosilicate glasses. *Bull. Russ. Acad. Sci. Phys.* 2019. **83**, No 3. P. 277–281. <https://doi.org/10.3103/S1062873819030158>.
43. Sakirzanovas S., Katelnikovas A., Dutczak D., Kareiva A. and Jüstel T. Concentration influence on temperature-dependent luminescence properties of samarium substituted strontium tetraborate. *J. Lumin.* 2012. **132**, No 1. P. 141–146. <https://doi.org/10.1016/j.jlumin.2011.08.011>.
44. Edgar A., Varoy C.R., Koughia C. *et al.* High-resolution X-ray imaging with samarium-doped fluoroaluminate and fluorophosphate glass. *J. Non-Cryst. Solids*. 2013. **377**. P. 124–128. <https://doi.org/10.1016/j.jnoncrysol.2012.12.022>.
45. Babu B.H., Kumar V.V.R.K. Fluorescence properties and electron paramagnetic resonance studies of γ -irradiated Sm³⁺ doped oxyfluoroborate glasses. *J. Appl. Phys.* 2012. **112**, No 9. P. 093516. <https://doi.org/10.1063/1.4764043>.
46. Nogami M. and Abe Y. Fluorescence properties of Sm²⁺ ions in silicate glasses. *J. Appl. Phys.* 1996. **80**, No 1. P. 409–414. <https://doi.org/10.1063/1.362770>.
47. Wang J., Huang Y., Li Y., Seo H.J. The reduction and luminescence characteristics of Sm²⁺ doped in Ba₃BP₃O₁₂ crystal. *J. Am. Ceram. Soc.* 2011. **94**, No 5. P. 1454–1459. <https://doi.org/10.1111/j.1551-2916.2010.04250.x>.
48. Rao B.V., Kumar R.J. and Rao K.V. Concentration quenching effects in samarium doped zinc phosphate glasses for visible applications. *Int. J. Pure Appl. Phys.* 2017. **13**, No 3. P. 301–316.
49. Campbel I.H. and Fauchet P.M. The effects of microcrystal size and shape on the one phonon Raman spectra of crystalline semiconductors. *Solid State Commun.* 1986. **58**, No 10. P. 739–741. [https://doi.org/10.1016/0038-1098\(86\)90513-2](https://doi.org/10.1016/0038-1098(86)90513-2).
50. Viera G., Huet S., Boufendi L. Crystal size and temperature measurements in nanostructured silicon using Raman spectroscopy. *J. Appl. Phys.* 2001. **90**, No 8. P. 4175–4183. <https://doi.org/10.1063/1.1398601>.
51. Rani E., Ingale A.A., Chaturvedi A. *et al.* Correlation of size and oxygen bonding at the interface of Si nanocrystal in Si–SiO₂ nano-composite: A Raman mapping study. *J. Raman Spectrosc.* 2016. **47**, No 4. P. 457–467. <https://doi.org/10.1002/jrs.4832>.

Authors and CV



Katerina V. Michailovska, PhD in Physics and Mathematics, Senior Researcher at the V. Lashkaryov Institute of Semiconductor Physics, NASU. Authored 169 publications, 15 patents, 1 monograph. The area of her scientific interests is physics (optic, luminescence) of thin-film semiconductor structures and nano-sized systems based on them. E-mail: k_mich@ukr.net, <http://orcid.org/0000-0001-6088-7123>



Ivan Z. Indutnyi, Doctor of Physics and Mathematics, Professor, Chief Researcher at the V. Lashkaryov Institute of Semiconductor Physics. His main research activity is in the field of optics of thin films, photostimulated processes in solids and on their surfaces, nanoparticles and nano-structures, interference lithography, plasmonics and sensing. Author of more than 300 publications, 35 author’s certificates and patents. E-mail: indutnyy@isp.kiev.ua, <http://orcid.org/0000-0002-7088-744X>



Petro Shepeliavyi, PhD in technical sciences, senior research scientist at the V. Lashkaryov Institute of Semiconductor Physics, NASU. His field of scientific interests includes: inorganic resists and their application in lithography, holography, optical engineering, information recording, absorbing metal-dielectric coatings, *etc.* He is the author of more than 250 publications, 40 author’s certificates and patents. E-mail: spe@isp.kiev.ua, <http://orcid.org/0000-0002-4119-1099>



Mykola V. Sopinsky, PhD in Physics and Mathematics, Senior Researcher at the V. Lashkaryov Institute of Semiconductor Physics. The area of his scientific interests – interference lithography, photo- and thermostimulated processes in thin-film structures, plasmonics, synthesis and characterization of nano-materials, ellipsometry. He is the author of more than 140 publications. E-mail: sopinsky@ua.fm, <http://orcid.org/0000-0002-0101-1241>



Viktor A. Dan'ko, Doctor of Physics and Mathematics, Leading Researcher of the V. Lashkaryov Institute of Semiconductor Physics, NAS of Ukraine. His main research activity is in the field of optics of thin films, photostimulated processes in thin film structures, nanoparticles and nanostructures, interference lithography. He is the author of more than 150 publications, 11 patents. E-mail: danko-va@ukr.net, <http://orcid.org/0000-0001-8106-3182>



Volodymyr O. Yukhymchuk, Professor, Doctor of Sciences, Head of the Department at the V. Lashkaryov Institute of Semiconductor Physics, NAS of Ukraine. The area of his scientific interests includes Raman spectroscopy, luminescence, quantum dots, semiconductors, nanostructures. E-mail: v.yukhymchuk@gmail.com, <http://orcid.org/0000-0002-5218-9154>

Authors' contributions

Michailovska K.V.: idea, methodology research, visualization, writing the first original version of the article.

Indutnyi I.Z.: conceptualization, methodology, review and editing.

Shepeliavyy P.E.: methodology, production of original samples for research, discussion.

Sopinsky M.V.: visualization, writing – review, discussion and editing.

Dan'ko V.A.: research, formal analysis, discussion and editing.

Yukhymchuk V.O.: methodology, research, analysis of the results, discussion and editing.

Люмінесцентні та Раманівські дослідження структур, сформованих при відпалі плівок $\text{SiO}_x\text{:Sm}$

К.В. Михайловська, І.З. Індутний, П.С. Шепелявий, М.В. Сопінський, В.А. Данько, В.О. Юхимчук

Анотація. Досліджено вплив домішок самарію на процеси високотемпературного розкладу в плівках SiO_x , легованих самарієм під час термічного співвипаровування у вакуумі монооксиду кремнію та металевого Sm. Високотемпературний відпал плівок $\text{SiO}_x\text{:Sm}$ в атмосфері повітря приводить до формування структур ncs-Si-SiO_x:Sm. Шляхом вивчення спектрів фотолюмінесценції (ФЛ) нанокompозитів ncs-Si-SiO_x:Sm було показано, що легування плівок SiO_x самарієм прискорює їх розпад на Si і SiO_2 при термічному відпалі, а також знижує температуру переходу наночастинок кремнію з аморфного стану у кристалічний. Зі збільшенням вмісту домішок Sm у ncs-Si-SiO_x:Sm до 2 мас.%, поряд зі ФЛ, пов'язаною з наночастинками кремнію, у спектрі ФЛ цих структур з'являються смуги випромінювання іонів Sm^{3+} та Sm^{2+} , які не спостерігаються при менших концентраціях Sm. Наявність нанокристалів кремнію у плівках SiO_x , легованих Sm і відпалених при 970 °C у повітрі, підтверджено спектрами комбінаційного розсіювання. Обговорено можливий механізм взаємодії іонів самарію з матрицею SiO_x і ncs-Si.

Ключові слова: наночастилки кремнію, нанокompозити кремнію, рідкоземельні елементи, фотолюмінесценція, спектри КРС, самарій.